Microwave land emissivity calculations using AMSU measurements

Fatima KARBOU

CNRS / IPSL / CETP, France

Catherine PRIGENT

CNRS / Observatoire de Paris / LERMA, France

Laurence EYMARD

CNRS / IPSL / LODYC, France

Juan PARDO

Inst. Estructura de la Materia / DAMIR, Spain

April 29, 2004

Corresponding author :

Fatima KARBOU

10-12 , Avenue de l'Europe

78140, Vélizy, France

email: fatima.Karbou@cetp.ipsl.fr

Tel. + 33 1 39 25 39 25

Fax. +33 1 39 25 47 78

Abstract- *Atmospheric parameter retrievals over land from AMSU measurements, such as atmospheric temperature and moisture profiles, could be possible using a reliable estimate of the land emissivity. The land surface emissivities have been calculated using 6 months of data, for 30 beam positions (observation zenith angles from –58° to +58°) and the 23.8, 31.4, 50.3, 89, and 150 GHz channels. The emissivity calculation covers a large area including Africa, Eurasia, and Eastern South America. The day-to-day variability of the emissivity is less than 2% in these channels. The angular and spectral dependence of the emissivity is studied. The obtained AMSU emissivities are in good agreement with the previously derived SSMI ones. The scan asymmetry problem has been evidenced for AMSU-A channels. And possible extrapolation of the emissivity from window channels to sounding ones has been successfully tested.*

Index Terms—AMSU, microwave surface emissivity.

1. INTRODUCTION

Passive microwave measurements from the Advanced Microwave Sounding Unit (AMSU) A and B on board the National Oceanic and Atmospheric Administration (NOAA) polar orbiting satellites are increasingly used over ocean in operational numerical weather prediction (NWP) models. The AMSU-A sounding channels are used for atmospheric temperature profile retrievals whereas the AMSU-B channels are designed for atmospheric humidity profiling. In addition, AMSU window channels are sensitive to the surface, cloud, and rain, and can be used to derive many parameters such as total precipitable water, sea ice concentration, precipitation rate, or cloud liquid water [*Grody et al*., 2001, *Zhao and Weng*, 2002].

However, AMSU profiling information is still insufficiently exploited over land. The land surface emissivity is high (often close to 1.0) as compared to the ocean one and experiences strong temporal and spatial variations with surface types, roughness, and moisture content, among other parameters. Consequently, it is more difficult to discriminate between the surface and atmosphere contributions over land than over ocean. So far, only the profiling channels that are not sensitive to the surface are operationally used over land. *English* [1999] showed that the use of land emissivity with an accuracy better than 2% would help humidity profile retrievals over land. The present study is essentially motivated by the need to improve the low level atmospheric temperature and humidity profiles retrievals over land. It is crucial to estimate accurate land surface emissivities at a global scale for the AMSU channels in order to allow accurate retrievals of the temperature and humidity in the lower atmospheric layers.

Various emissivity model developments have been conducted, but the modelling approaches for global applications are hampered by 1) the complexity of the interaction between the radiation and the large variability of the medium encountered over the globe; 2) the lack of accurate input parameters to feed the model (vegetation characteristics, soil moisture, roughness, among others). Ground based and aircraft measurements of land surface emissivities have been performed, but their extrapolation to surfaces at larger scales is questionable. Airborne microwave measurements have been used to estimate land surface emissivity of forest and agricultural areas [*Hewison*, 2001], and snow and ice surfaces [*Hewison and English*, 1999] at 24, 50, 89, and 150 GHz.

Land emissivity studies at regional to global scales have already been carried out directly from satellite measurements. *Prigent et al.* [1997, 1998] estimated the microwave land emissivities over the globe at the frequencies of the Special Sensor Microwave/Imager (SSMI) channels (19, 22, 35 and 85 GHz) for vertical and horizontal polarisations, at 53° zenith angle by removing the atmosphere, clouds, and rain

contributions using ancillary satellite data. Extrapolation of these estimates to AMSU-A frequencies and scanning conditions has been attempted [*Prigent et al.,* 2000]. Other emissivity calculations have been performed for limited geographic areas. *Felde and Pickle* [1995] retrieved surface emissivities at 91 and 150 GHz for cloud free data from SSM/T2 atmospheric water vapor profiler and radiosonde measurements. *Choudhury* [1993] calculated the surface reflectivity at 19 and 37 GHz using SSMI/I data over different surface types. *Jones and Vender Haar* [1997] proposed a method to routinely generate the microwave land emissivity, using microwave and infrared satellite data. *Morland et al.* [2001] used SSM/I data to compute surface emissivities in semi-arid areas. Similar surface types have been previously sensed using microwave aircraft observations to derive land surface emissivity from 24 GHz to 157 GHz [*Morland et al*., 2000].

The goal of this study is to calculate reference land surface emissivity maps at AMSU frequencies and scanning conditions, directly using AMSU observations. The procedures are to get the land emissivities at 23.8, 31.4, 50.3, 89, and 150 GHz for all AMSU zenith angles by removing the contribution of the atmosphere, clouds, and rain. The International Satellite Cloud Climatology Project (ISCCP) data is used to identify cloud-free AMSU observations and to provide an accurate value of the skin temperature [*Rossow and Garder*, 1991]. The European Centre for Medium-Range Weather Forecasts (ECMWF) temperature-humidity profiles are used to input the Atmospheric Transmission at Microwave (ATM, [Pardo et al., 2001]) radiative transfer model that calculates the cloud-free atmospheric contribution. Results are presented for 6 months of AMSU data in 2000, covering a large geographic area (from –60° to +60° in longitudes and latitudes). The emissivity retrieval scheme (data and method) for AMSU window channels is described in section 2 and an error analysis is conducted. The angular and spectral variations of the AMSU emissivities are characterized (section 3), and the day-to-day variability is briefly discussed. Extrapolation to the AMSU sounding channels is tested in Section 4. Section 5 provides the conclusions.

2. THE LAND SURFACE EMISSIVITY CALCULATION FOR AMSU WINDOW CHANNELS

2.1. The data

The AMSU sounding unit is operational on board the NOAA 15 satellite since 1998. It contains two modules A and B. The first one, AMSU-A measures the outgoing radiation from the Earth's surface and from different atmospheric layers using 15 spectral regions (23.8-89.0 GHz). The sounding channels (52.8 to 58 GHz) are used to retrieve the atmospheric temperature information from about 3 hPa (45 km) to the Earth's surface. AMSU-A is composed of two separate units: AMSU-A1 with 12 channels in the frequency range 50-60 GHz bands and one channel at 89 GHz, and AMSU-A2 unit with 2 surface channels at 23.8 and 31.4 GHz. Moreover, the AMSU-A1 unit benefits of 2 antenna

systems to provide measurements from 50 GHz to 89 GHz. AMSU-B is designed for humidity sounding and has two window channels at 89 and 150 GHz and three other channels centred on the 183.31 GHz water vapour line. AMSU A and B have a nominal field of view of 3.3° and 1.1° and sample 30 and 90 Earth views respectively. Thereby, the AMSU observation scan angle θ_s varies from –48° to +48°. Consequently, the corresponding local zenith angle could reach 58°. Channel characteristics for both AMSU-A and AMSU-B radiometers are given in Table I and a detailed description of the AMSU sounders is reported in *Goodrum et al.* [2000]. In the present study, level 1b AMSU data from year 2000 have been obtained from the Satellite Active Archive (SAA) and processed using the Advanced ATOVS Processing Package (AAPP) created and distributed by EUMETSAT and co-operations. The AMSU radiances are corrected from the AMSU antenna effect [*Mu*, 1999; *Hewison et al.*, 1996].

Clouds have a great impact on the observed microwave radiances. Therefore, cloudy situations should not be accounted for in the emissivity calculation. Cloud parameters and skin temperature are extracted from the ISCCP pixel level data (the DX data set) for year 2000. These parameters are available at 30 km ground resolution and every 3 hours. Within ISCCP, information about clouds are obtained from visible and infrared measurements from polar and geostationary satellites, using radiative analysis [*Rossow and Schiffer*, 1991]. Clear infrared radiances are then used to derive an accurate value of the skin temperature known to be the closest one to the physical surface temperature. The skin temperature accuracy is assumed to be within 4 K as reported by *Rossow and Garder* [1993a, b].

The cloud-free atmospheric contribution is calculated via radiative transfer simulations using as input the ECMWF temperature-humidity profiles. The profiles we used are from the ECMWF ERA40 re-analysis for 2000 available globally, every 6 hours, for 60 vertical pressure levels, and for a horizontal grid resolution of 1.125°x1.125°.

2.2. The emissivity calculation

In the AMSU microwave frequencies range, for a non scattering plane-parallel atmosphere and, for a given path zenith angle, the brightness temperature observed by the satellite instrument can be expressed as:

$$T_{b(p,\upsilon)} = T_{skin} \times \varepsilon_{(p,\upsilon)} \times \Gamma + T_{(\upsilon,\downarrow)} \times (1 - \varepsilon_{(p,\upsilon)}) \times \Gamma + T_{(\upsilon,\uparrow)} \quad (1)$$

$$\Gamma = e^{-\tau(0,H)/\cos(\theta z)} \quad (2)$$

$T_{b\,(p,\upsilon)}$ and $\varepsilon_{(p,\upsilon)}$ are the instrument brightness temperature and the surface emissivity at frequency υ and for polarisation p, respectively. T_{skin}, $T_{(\upsilon,\downarrow)}$ and $T_{(\upsilon,\uparrow)}$ are the skin temperature, the upwelling and the downwelling brightness temperatures respectively. Γ is the net atmospheric transmissivity.

(1) leads to the land emissivity expression:

$$\varepsilon_{(p,\upsilon)} = \left(T_{b\,(p,\upsilon)} - T_{(\upsilon,\uparrow)} - T_{(\upsilon,\downarrow)} \times \Gamma \right) / \left(\left(T_{skin} - T_{(\upsilon,\downarrow)} \right) \times \Gamma \right) \quad (3)$$

For the emissivity estimation, we took into account all AMSU cloud-free observations and all AMSU-A zenith angles (30 values from –58° to +58°). The radiative transfer computations are performed using the ATM model. This model, based on different developments and measurements described in [*Pardo et al.*, 2001], is fully applicable in the 0-1600 GHz frequency range and has been evaluated by inter-comparisons with other existing radiative transfer models [*Garand et al.*, 2001].

2.3. The emissivity sensitivity to errors in the input parameters

The accuracy of the estimated microwave emissivity to errors in the input parameters is evaluated by analysing its change due to a variation in one of them, the other parameters remaining unchanged. The accuracy evaluation is performed for 5 days of AMSU-A and B cloud-free data from early January 2000 and covers a large geographic area (Africa, Southern Europe, and Middle East) collocated with ECMWF temperature and humidity profiles, and ISCCP skin temperatures.

From (4), the input parameters involved in the emissivity estimation are: the skin temperature, the instrument brightness temperature, and the air humidity and temperature profiles. For example, the impact of humidity profile errors on the microwave emissivity is estimated by calculating the emissivity variation due to an alteration in the humidity profile. The emissivity change is then calculated as the difference between the emissivity obtained with two modified mixing ratio profiles (the first one increased by 15% for the 60 levels and the second one decreased by 15% for the 60 levels), the observed temperature profile, the skin temperature, and the instrument brightness temperature remaining unchanged. The same approach is used to determine the emissivity variation due to the air temperature profile (+/- 1 K at all pressure levels), to the instrument brightness temperature (+/- 1 K), and to the skin temperature (+/- 4 K). The emissivity variations are calculated at 23.8, 31.4, 50.3, 89, and 150 GHz, for four observation classes: (a) low zenith angles (<45°), (b) high zenith angles (> 45°), (c) dry atmospheres (Total Water Vapour Content (TWVC) < 30 Kg/m^2), and (d) moist conditions (TWVC >30 Kg/m^2). The corresponding results are given in Table2. Similar results are obtained analytically for the surface temperature and instrument brightness temperature. Calculations are not shown for the other AMSU frequencies that are located near the oxygen and water vapor lines. At these frequencies with low atmospheric transmission, the surface contribution to the measured radiation is not large enough to provide reliable emissivity estimates. In the following

section, the emissivity frequency dependence will be discussed and a solution will be provided and tested to estimate the emissivities in these opaque channels from the near-by window frequency observations.

Table 2 shows that for all window channels, the emissivity decreases when the air mixing ratio, the surface temperature, or air temperature increases. On the contrary, an increase in the instrument brightness temperature enhances the estimated emissivity. At all frequencies, the emissivity variation due to errors in one input parameter is larger for high TWVC and for high observation zenith angles: this is explained by the fact that increasing TWVC as well as increasing zenith angle result on a decrease in the atmospheric transmissivity and, therefore, less sensitivity to the surface contribution. Errors in the humidity profiles have little effects on the surface channels 23.8, 31.4 and 50.3 GHz (less than 0.25% of relative error ($d\varepsilon/\varepsilon$)). However, their impact is greater on the 89 and 150 GHz emissivities: in dry atmospheres or for low zenith angles, the emissivity sensitivity is five times greater at these two channels than at the 23.8 GHz one. This effect is enhenced for very moist conditions and large zenith angles, with errors rising up to 1.1% at 89 GHz and 4% at 150 GHz. Errors in skin temperatures greatly influence the retrieved emissivity at all frequencies. For dry conditions, the emissivity relative errors are about 3% for 23.8 and 31.4 GHz, 3.5% at 50 and 89 GHz, and 4% at 150 GHz. These errors increase with increasing TWVC and zenith angles. As expected, errors in the air temperature profile produce larger emissivity variations at 50 GHz than at other frequencies that are located farther away from the oxygen absorption bands.

In order to reduce the calculation errors, the emissivity calculations will be averaged over a certain period of time. The time variability will be analysed and compared to the theoretical noise errors previously calculated. Note that contrarily to SSM/I observations, AMSU measurements are performed at various incidence angles, thus limiting the number of overpasses per location with the same observation conditions.

3. AMSU LAND EMISSIVITY ANALYSIS

3.1. EMISSIVITY MAPS

Monthly mean emissivity maps are shown on Figure 1.a and 1.b, at 23.8 and 89 GHz respectively, for July 2000, averaged over zenith angles lower than 45°. All available cloud-free AMSU observations are used to produce these maps at a 30x30 km resolution. The corresponding emissivity standard deviation maps are also presented (Figure 1.c and 1.d).

The monthly mean emissivity maps show expected spatial structures, related to changes in surface types. Lakes and rivers as well as the coastlines are associated with low emissivities at all frequencies. Compared to other medium, water has high dielectric values that translate into low emissivities. The Victoria, Malawi, and Tanganyika lakes are easily distinguished. Open water areas are also associated with the highest emissivity variability (see Figure 1.c and 1.d). At the border between land and open water, the percentage of each contribution (land and water) can change between two satellite overpassings because they are not perfectly coincident in space, leading to significant emissivity changes. The emissivity also changes with vegetation cover. We used the Biosphere-Atmosphere Transfer Scheme (BATS) vegetation land cover data set (available at 30x30 km grid resolution) for vegetation classification [*Dickinson et al.*, 1986]. Table 3 lists the different vegetation classes available in the dataset and figure 2 shows the geographic distribution of the vegetation classes. Bare soil areas (like desert regions in North Africa and Arabia) are characterized by lower emissivity. They have a quasi-specular behaviour. On the other hand, dense vegetation areas have a quasi-lambertian reflection associated to rather high emissivity. This is confirmed by the emissivity histograms calculated using February 2000 data at 23.8, 31.4, 50.3, and 89 GHz (Figure 3.a, 3.b, 3.c and 3.d respectively). The histograms are established for two zenith angle classes (angles <= 45° and angles > 45°) and for desert and dense vegetation areas (see Figure 3a-d). As expected, and for all frequencies, the emissivity is higher at low zenith angles than at higher ones for desert areas. The emissivity change due to the zenith angle (difference between the mean emissivity for low angles and the mean emissivity for high angles) is about 0.024 for 23.8 and 31.4 GHz and 0.023 for 50.3 and 89 GHz. The emissivity change for a dense vegetation area is smaller: less than 0.009 for channels 1 and 2 and about 0.01 for the two others. We examine in detail the emissivity variation depending on zenith angle in the next section. In the desert, two particular areas of very low emissivities will be noted, one in the South of Arabia (Western Oman, Eastern Yemen) and another one in Egypt. These regions also show low emissivities on the maps derived from SSM/I observations. They have been showed to be related to geological structures [*Prigent et al.*, 2003] but no final explanation exists yet despite on-going assiduous investigations (dielectric measurement of rocks and sand from those regions along with modelling studies).

3.2. DAY-TO-DAY EMISSIVITY VARIATIONS

As shown by Figure 1c & 1d, the day-to-day emissivity standard deviations for 1 month are generally within 0.02 for all channels, i.e. within the required theoretical limit calculated by *English* [1999]. As expected, they tend to increase with frequency, given the increasing sensitivity to atmospheric contamination and sensitivity to surface temperature errors (see section 2.3). As already discussed, areas with higher variations are often associated with the presence of standing water (coastal areas, flood regions). For the month of July shown here (Figure 1), the subsahelian transision zone in Africa

is associated with rather large emissivity variations. This fact is likely related to the rainy season in this region at this period of the year with two consequences: 1) potential cloud contamination is likely, 2) rain-induced soil moisture variation along with the corresponding vegetation changes can lead to important emissivity variations.

In order to further evaluate the day-to-day variation of the estimated emissivity, two areas with different vegetation cover have been selected. We calculate for them the mean daily emissivity during the month of January 2000 at 23.8, 31.4, 50.3, 89, and 150 GHz. To avoid the emissivity variation due to the zenith angles, data at angles less than 45° are selected. Moreover, all water pixels (lakes and rivers) are removed for the calculation to avoid the emissivity change between land and water surfaces. The calculation results are shown on Figure 4 (a-f). Figures 4a, c and e show the day-to-day variation of the emissivity over a desert area in Mauritania (15W 10W; 20N 25N) at 23.8, 89 and 150 GHz respectively. The mean emissivity curve has the same trend for all frequencies. Error bars are larger for 89 and 150 GHz, which is consistent with the error analysis of the previous section. The emissivity variation is not only due to errors in the input parameters: it can also correspond to real changes in surface properties. Between day 15 and day 20, a significant emissivity decrease can be observed. We checked on the ISCCP cloud data set that it corresponds to the overpassing of a significant convective activity in the region, likely associated to rain and induced soil moisture increase. Figures 4b, d, and f present the day-to-day variation of the emissivity over a tropical forest in Africa (18W 10W; 0N 10N) at 23.8, 89, and 150 GHz, respectively. For all channels (except the 150 GHz), the emissivity remains almost unchanged during the month. At 150 GHz, the emissivity is associated with large daily variability that can be related to the sensitivity of this channel to input errors especially for high TWVC situations.

3.3.ANGULAR DEPENDENCE OF THE AMSU EMISSIVITY

The cross-track scanning pattern of the AMSU instrument provides observation angles between +/- 58°. In addition, because of the rotating AMSU antenna, the estimated emissivity is a mixture between the vertical and the horizontal polarizations. The AMSU emissivity at scan angle θ_z could be written as follows:

$$\varepsilon(\theta_z) = \varepsilon_p(\theta_z)\cos^2(\theta_s) + \varepsilon_q(\theta_z)\sin^2(\theta_s) \quad (4)$$

Where:

$\varepsilon_p(\theta_z)$ and $\varepsilon_q(\theta_z)$ are the two orthogonal polarized surface emissivities at θ_z local zenith angle. For AMSU surface channels, the polarization is vertical near nadir and thereby, ε_p is equal to ε_v and εq is equal to ε_h.

In order to examine the emissivity variation with the zenith angle, the calculated emissivities have been sorted by beam position and vegetation type (nadir corresponds to scan positions 15 and 16). The

resulting monthly mean emissivities for vegetation class 8 (desert) and vegetation classes 6 and 7 (dense vegetation) are presented on figure 5 for January and August 2000. Regarding each vegetation class, SSMI emissivities for January 1993 and August 1992 (obtained from *Prigent et al.* [1997]) at 19, 37 and 85 GHz and for 53° zenith angle (scan positions 2 and 29), recalculated for an AMSU like polarization (using equation 4) are added to the plots for comparison. For example, at 23.8 GHz, we add the estimated SSMI emissivity at 19 GHz for 53°. For both vegetation types and for all channels, we notice a very good agreement between the AMSU emissivities at zenith angles close to 53° and the SSMI ones. The figure shows the strong dependence of the AMSU emissivity with the zenith angles over desert areas. We observe the same behaviour over semi-desert areas (see figure 6 for vegetation class 11). For forested areas, the dependence is much smaller, as expected: dense vegetation is associated with quasi-lambertian reflection and thereby the observation angle has a limited impact. Additional plots using January data are provided on figure 6, for 9 vegetation classes and for all surface channels (23-150 GHz).

The results show also an asymmetry along the AMSU scan, relatively to nadir, variable with frequency and surface emissivity. To highlight this effect, we have calculated the difference between the monthly mean emissivities at the scan edges (scan positions 1 and 30) for different vegetation covers, for 6 months of data, at 23.8, 31.4, 50.3, and 89 GHz (see figure 7). For all surfaces, the asymmetry (monthly mean emissivity at scan position 30 minus the monthly mean emissivity at scan position 1) is always positive for 23.8 and 31.4 GHz (both channels are located on the AMSU-A1 module) and always negative for 50.3 and 89 GHz (measurements at these frequencies are obtained from the AMSU-A2 module). For all vegetation classes, the AMSU scan asymmetry is higher at 31.4 GHz than at the other frequencies. The maximum bias at this frequency is about 0.033 and is observed over desert surfaces (surface with the lowest emissivity). Notice that 0.033 in emissivity scan asymmetry could represent 9 K in terms of brightness temperature (assuming a skin temperature of 300 K and an atmospheric transmissivity of 0.9). Channel 2 (23.8 GHz) is located on the same module (AMSU-A1) than channel 1 (31.4 GHz), but is less sensitive to the asymmetry; the maximum asymmetry is less than 0.024. Measurements at 89 GHz appear to be less sensitive to the scan asymmetry than those at 50.3 GHz. [*Weng et al.*, 2003] also noticed an asymmetry in the AMSU 31GHz channel by using observations over an ocean background surface. The AMSU scan asymmetry could be related to an instrument problem. For performant retrievals of atmospheric parameter over ocean and land, the instruments have to be accurately calibrated for all conditions (frequencies and scanning positions). Further studies should investigate this asymmetry problem over land and ocean surfaces to suggest adequate corrections.

3.4.FREQUENCY DEPENDENCE OF THE AMSU EMISSIVITY

Figure 8 shows the monthly mean emissivities for dry and vegetated surfaces calculated using January data, at AMSU window channels between 23.8 and 150 GHz and for high (>45°) and low (≤ 45°) zenith angles. For comparison purposes, SSMI emissivities at 19, 3,7 and 85 GHz, at 53° for January 1993 are added to the plots (using the polarization mixing from equation 4). For bare soil (figure8.a, 8.b) and vegetated areas (figure 8.c and 8.d), the frequency dependence of the AMSU emissivities at high zenith angles is in very good agreement with the ones derived from SSM/I estimates. For all considered vegetation classes and both high and low zenith angles, the emissivity slightly decreases from 23 to 31 GHz and then increases at 50 GHz. The amplitude of the increase at 50 GHz does not depend significantly upon scan angle or TWVC (similar trend over desert and tropical forest). This could be due at least to two factors: absolute instrument calibration error at 50 GHz, systematic errors in the gaseous absorption calculation at this frequency. Additional investigations have to be performed, both over ocean and land to understand this problem. At 23.8, 31.4 and, 50 GHz, error bars have the same magnitude for low zenith angles and for all surface types and are smaller than at 89 and 150 GHz. For all channels, the error bars increase with increasing zenith angles. The channels 89 and 150 GHz are more sensitive to residual atmospheric errors leading to increasing error bars; this effect is intensified at 150 GHz for moist conditions and high zenith angles. The observed emissivity decreases in vegetated areas at high zenith angles between 89 and 150 GHz is not realistic. In section 2.3, it has been shown that the 150 GHz channel is particularly sensitive to errors in all calculation input parameters. This is also evidenced by the large error bars associated with the emissivity estimates at this frequency (almost 0.07 for vegetation class 7 as compared to 0.03 for the other frequencies). For low zenith angles, the emissivity does not change much from 89 and 150 GHz for both dry and vegetated areas: the emissivity estimate at 150 GHz being very noisy, emissivity estimates at 89 GHz could be used for the 150 GHz channel, at least for low zenith angle. We have checked this assumption in the next section by using emissivities at 89 GHz to calculate the brightness temperature at 150 GHz.

4. EXTRAPOLATION OF THE CALCULATED LAND SURFACE EMISSIVITIES TO THE SOUNDING CHANNELS

The emissivity calculations have been performed and analysed for the AMSU window channels. As already mentioned, similar calculations for sounding channels would not be adequate, due to low atmospheric transmission that translates into limited contribution of the surface radiation at these frequencies. Even the 150 GHz channel calculations have been shown rather noisy as compared to the other window channels, due to lower atmospheric transmission.

Could the emissivities in the sounding channels be accurately estimated from the closest window channels? Simulating the brightness temperatures in the sounding channels using the averaged emissivities calculated in the closest window channel tests this assumption. For comparison purposes, the mean emissivities in the window channels are calculated for the even days in January 2000 for incidence angles lower that 45°, and the brightness temperatures are also calculated for the window channels for the odd days for the same window frequencies, using the mean emissivities estimated from the even days. That way, the errors derived from the frequency extrapolation will be compared to the natural errors observed for the corresponding frequency. Figure 9 shows the scatter plots of the observed brightness temperatures for the odd days in January for 9 AMSU frequencies versus the simulated brightness temperatures using the ATM radiative transfer code, the corresponding ECMWF atmospheric profiles and ISCCP surface temperature, and the mean emissivities calculated in the window channels for the even days for the same month. The simulated brightness temperatures at channels 52.8 and 53 GHz use the emissivity calculated at 50 GHz and similarly, the emissivity calculated at 150 GHz is used for the simulations at 183.31+/-7. Good agreements are observed between the measured and the simulated brightness temperatures for all channels, and the agreement is particularly remarkable in the sounding channels. The Root Mean Square errors at window channels are less than 4 (3.44, 3.93, 2.63, 3.80, and, 3.24 at 23.8, 31.4, 50, 89 and, 150 GHz). Good results are obtained for the sounding channels: an RMS of ~ 2 for channels 52 and 53 GHz, and 3.64 for the 183±7 GHz channel.

The present results show that the emissivity calculation scheme produces quite good estimates of the AMSU brightness temperatures. The radiative transfer model generates a very realistic estimation of the atmospheric contribution since the results for channels less sensitive to surface are also very consistent. For example the RMS errors at AMSU channels 6, 7, 8, 9, 11, and 12 are 1.41, 1.03, 0.38, 0.45, 1.69, 0.61, and 0.71 respectively.

Given that the 150 GHz emissivity calculations are noisy compared to other surface channels, a further test is performed using the 89 GHz to simulate the brightness temperature at 150, 183+/-7 and 183+/-3 GHz. The corresponding results are given on figure 10. The RMS errors at 150 and 183±7 GHz are then 3.56 and 3.61 respectively.

Emissivity from the 150 GHz channel is noisier in moist month like July than in January. Figure 11 compares the obtained brightness temperature for 150 and 183.31±7, 183.31±3 and, 183.31±1 GHz channels for the 15 first days of August 2000 using emissivity at 89 GHz estimated with July 2000 data. The agreement between the observed and the simulated brightness temperatures is very good. The use of the emissivity at 89 GHz is a good approximation for the AMSU-B channels (150, 183.31+/-7, 183.31+/-3 GHz). This approximation allows us to avoid noise introduced by the 150 GHz retrieved emissivity, which is particularly important in very moist conditions and high zenith angles.

CONCLUSION

The land surface emissivities have been calculated for AMSU window channels for all scanning conditions, for six months in 2000, over Africa, Southern Europe, and the Middle East. The calculation makes use of an up-to-date radiative transfer model (ATM) and is performed for cloud-free AMSU observations. Ancillary data include the ISCCP cloud flags and surface skin temperature, along with the temperature and water vapor profiles from the ECMWF re-analysis. Emissivity maps are presented and show the realistic spatial variations with surface characteristics changes related to vegetation and the presence of open water. The day-to-day variability of the emissivities within a month is lower than 0.02 for all window channels, for low incidence angles. The angular and spectral dependence of the AMSU emissivity is examined for various surfaces. An instrumental AMSU-A problem is evidenced related to an asymmetry in the scan angle behaviour. For low incidence angles, the land surface emissivities in the sounding channels (50-60 GHz and 150-183 GHz) could successfully be extrapolated from the calculation in the closest window channels. In a following study, a parameterisation of the frequency and angular dependence of the emissivities will be proposed, anchored on accurate emissivity calculations directly derived from satellite observations at 23-89 GHz frequencies and at all incidence angles. The emissivity study is essentially motivated by the need to improve low level temperature and humidity profiles retrievals over land. The use of the AMSU window emissivities to retrieve atmospheric temperature and humidity information over land using AMSU-A and B measurements have been tested by *Karbou et al*. [2004]. The preliminary results are encouraging: the use of a reliable land emissivity information helps low level temperature and humidity profiles retrievals over land (about 2° and 7.5% of temperature and relative humidity RMS errors near the surface, respectively). Further details and investigations about this study will be proposed soon.

The emissivity resulting datasets for AMSU window channels and over Africa, Eurasia and Eastern South America are available for use by the scientific community. Moreover, further calculations are now conducted to enlarge the geographic area to the globe.

Acknowledgments-

The authors wish to thank Sophie CLOCHE and Jean Louis MONGE for their help to archive and process the ERA40 and AMSU data. They would like to thank Frederic CHEVALLIER and Fuzhong WENG for valuable discussions regarding AMSU calibration. The ISCCP data have been kindly provided by Bill ROSSOW.

REFERENCES

Choudhury, B.J., 1993, Reflectivities of selected land surface types at 19 and 37 GHz from SSM/I observations, *Remote Sensing of Environment*, Volume 46, Issue 1, pp. 1-17.

Dickinson, R.E., Henderson-Sellers, A., Kennedy, P.J., and Wilson, M.F., 1986, Biosphere-atmosphere transfer scheme (BATS) for the NCAR community climate model: NCAR Technical Note NCAR/TN275+STR, Boulder, CO. 69 p.

English, S., 1999, Estimation of temperature and humidity profile information from microwave radiances over different surface types, *J. Appl. Meteorol*., vol. 38, pp. 1526-1541.

Felde, G.W., and J. D. Pickle, 1995, Retrieval of 91 and 150 GHz Earth surface emissivities, *J. Geophys. Res*.,vol. 100, NO. D10, pp 20,855-20,866, Oct 1995.

Ferraro, R.R., F. Weng, N. Grody, and A. Basist, 1996: an eight year (1987-1994) time series of rainfall, clouds, water vapor, snow and sea ice derived from SSM/I measurements, *Bull. Amer. Meteor. Soc*., 77, 891-905.

Garand, L., D. S. Turner, M. Larocque, J. Bates, S. Boukabara, P. Brunel, F. Chevalier, G. Deblonde, R. Engelen, M. Hollingshead, D. Jackson, G. Jedlovec, J. Joiner, T. Kleespies, D. S. McKague, L. McMillin, J.-L. Moncet, J. R. Pardo, P. J. Rayer, E. Salathe, R. Saunders, N. A. Scott, P. Van Delst, and H. Woolf. 2001, Radiance and Jacobian intercomparison of radiative transfer models applied to HIRS and AMSU channels. *J. Geophys. Res*., 106, 24017-24031.

Goodrum, .G, K. B. Kidwell and W. Winston 2000, NOAA KLM user's guide. National Oceanic and Atmospheric Administration.

Grody, N.C., 1991, Classification of snow cover and precipitation using Special Sensor Microwave Imager (SSM/I), *J. Geophys. Res*., 96, 7423-7435.

Hewison, T.J., 2001, Airborne measurements of forest and agricultural land surface emissivity at millimetre wavelengths, *IEEE Trans. On Geoscience and Remote sensing*, V39, 2, 393-400.

Hewison, T.J., and S. English, 1999, Airborne retrieval of snow and ice surface emissivity at millimetre wavelengths, *IEEE Trans. On Geoscience and Remote sensing*, V37, 4, 1871-1879.

Hewison, T. J., and R. W. Saunders, 1996, Measurements of the AMSU-B Antenna Pattern, *IEEE Trans. On Geoscience and Remote sensing*, V34, 2, 405-412.

Jones, A. S., and T. H. Vonder Haar, *1997*, Retrieval of microwave surface emittance over land using coincident microwave and infrared satellite measurements , *J. Geophys. Res*.,vol. 102, NO. D12, pp 13,609-13,626, Jun 1997.

Karbou, F., F. Aires, C. Prigent, L. Eymard et J. Pardo, 2004, Atmospheric temperature and humidity profiles over land from AMSU-A and AMSU-B data, *Microrad04*, Roma, Italy.

Mo, T., 1999, AMSU-A Antenna Pattern corrections, *IEEE Trans. On Geoscience and Remote sensing*, V37, 1, 103-112.

Morland, J.C., David I. F. Grimes and T. J. Hewison, 2001, Satellite observations of the microwave

emissivity of a semi-arid land surface, *Remote Sensing of Environment*, Volume 77, Issue 2, pp. 149-164.

Morland, J.C., David I. F. Grimes, George Dugdale and Tim J. Hewison, 2000, The Estimation of Land Surface Emissivities at 24 GHz to 157 GHz Using Remotely Sensed Aircraft Data, *Remote Sensing of Environment*, Volume 73, Issue 3, pp. 323-336.

Pardo, J.P., J. Cernicharo and E. Serabyn, 2001, Atmospheric Transmission at Microwave (ATM): an improved model for millimetre/submillimeter applications, *IEEE Trans. Ant and Prop*, vol. 49, NO. 12, pp. 1683-1694.

Prigent, C., J.-Munier, G. Ruffié, and J. Roger, Interpretation of passive microwave satellite observations over Oman and Egypt, EGS-AGU, Nice, 2003.

Prigent, C., J.P. Wigneron, B. Rossow and J.R. Pardo, 2000, Frequency and angular variations of land surface microwave emissivities: can we estimate SSM/T and AMSU emissivities from SSM/I emissivities?, *IEEE trans. Geosci. Remote Sensing*, vol. 38, NO. 5, pp. 2373-2386.

Prigent, C., W.B. Rossow, and E. Matthews, 1998, Global maps of microwave land surface emissivities: potential for land surface characterization, *Radio Sci*., vol. 33, pp. 745-751.

Prigent, C., W.B. Rossow, and E. Matthews, 1997, Microwave land surface emissivities estimated from SSM/I observations, *J. Geophys. Res*., vol. 102, pp. 21 867-21 890.

Rossow, W.B. and L.C. Garder, 1993a, Cloud detection using satellite measuremenst of infrared and visible radiances for ISCCP, *J. Clim*., 6, 2341-2369.

Rossow, W.B. and L.C. Garder, 1993b, Validation of ISCCP Cloud detection, *J. Clim*., 6, 2370-2393.

Rossow, W. B. and R. A. Schiffer, 1991, ISCCP cloud data products, *Bull. Am. Meteor. Soc*., 72, pp. 2-20.

Weng, F., L. Zhao, R. Ferraro, G. Poe, X. Li, N. Grody, 2003: Advanced Microwave Sounding Unit Cloud and Precipitation Algorithms. Radio Sci., 38, 8,086-8,096.

Weng, F., B. Yan and N. Grody, 2001, A microwave land emissivity model, *J. Geophys. Res*., vol. 106, NO. D17, pp 20,115-20,123.

Zhao, L. and F. Weng, 2002, Retreival of ice cloud parameters using the Advanced Microwave Sounding Unit (AMSU), *J. Appl. Meteor*., 41, 384-395.

Table 1: AMSU-A/B Channel Characteristics

Channel No	Frequency (GHz)	Sensitivity (K)	Resolution at nadir (km)
AMSU-A			
1	23.8	0.20	48
2	31.4	0.27	48
3	50.3	0.22	48
4	52.8	0.15	48
5	53.596+/- 0.115	0.15	48
6	54.4	0.13	48
7	54.9	0.14	48
8	55.5	0.14	48
9	57.290=f_0	0.20	48
10	f_0 +/- 0.217	0.22	48
11	f_0 +/- 0.322 +/- 0.048	0.24	48
12	f_0 +/- 0.322 +/- 0.022	0.35	48
13	f_0 +/- 0.322 +/- 0.010	0.47	48
14	f_0 +/- 0.322 +/- 0.0045	0.78	48
15		0.11	48
AMSU-B			
16	89	0.37	16
17	150	0.84	16
18	183.31 +/- 1	1.06	16
19	183.31 +/- 3	0.70	16
20	183.31 +/- 7	0.60	16

Table 2: AMSU emissivity sensitivity to: (a) errors in the air humidity profiles, (b) errors in the air temperature profiles, (c) errors in the skin temperature, and (d) errors in the instrument brightness temperature

Frequencies (GHz)	θ <= 45° 30200 points	θ > 45° 6886 points	TPW <= 30 g/m² 26472 points	TPW > 30 g/m² 10616 points
	(a) Air humidity errors (mean/std)			
23.8	-0.001 / 0.001	-0.002 / 0.002	-0.001 / 0.001	-0.001 / 0.003
31.4	-0.001 / 0.001	-0.002 / 0.002	-0.001 / 0.001	-0.003 / 0.003
50.3	-0.001 / 0.001	-0.002 / 0.002	-0.001 / 0.001	-0.003 / 0.004
89.0	-0.005 / 0.005	-0.009 / 0.008	-0.006 / 0.004	-0.010 / 0.014
150	-0.004 / 0.015	-0.006 / 0.035	-0.007 / 0.012	0.023 / 0.056
	(b) Air temperature errors (mean/std)			
23.8	-0.001 / 0.001	-0.001 / 0.001	-0.001 / 0.001	-0.002 / 0.001
31.4	-0.001 / 0.001	-0.001 / 0.001	-0.001 / 0.001	-0.001 / 0.001
50.3	-0.005 / 0.001	-0.010 / 0.001	-0.006 / 0.002	-0.008 / 0.003
89.0	-0.002 / 0.001	-0.003 / 0.003	-0.002 / 0.001	-0.008 / 0.004
150	-0.008 / 0.010	-0.017 / 0.027	-0.007 / 0.007	-0.045 / 0.036
	(c) Skin temperature errors (mean/std)			
23.8	-0.028 / 0.002	-0.029 / 0.002	-0.028 / 0.002	-0.031 / 0.002
31.4	-0.028 / 0.002	-0.027 / 0.002	-0.027 / 0.002	-0.028 / 0.002
50.3	-0.036 / 0.003	-0.041 / 0.004	-0.037 / 0.003	-0.038 / 0.004
89.0	-0.030 / 0.002	-0.031 / 0.004	-0.030 / 0.002	-0.035 / 0.004
150	-0.037 / 0.009	-0.042 / 0.016	-0.037 / 0.008	-0.062 / 0.017
	(d) Instrument brightness temperature errors (mean/std)			
23.8	0.008 / 0.001	0.009 / 0.001	0.0085 / 0.001	0.0106 / 0.001
31.4	0.008 / 0.001	0.008 / 0.001	0.0079 / 0.001	0.0085 / 0.001
50.3	0.015 / 0.002	0.021 / 0.003	0.0158 / 0.003	0.0177 / 0.004
89.0	0.010 / 0.002	0.012 / 0.004	0.0102 / 0.002	0.0173 / 0.005
150	0.024 / 0.027	0.054 / 0.102	0.0215 / 0.017	0.1378 / 0.151

Table 3: Biosphere-Atmosphere Transfer Scheme (BATS) Vegetation Classes

Classes	Legend	Total number of selected AMSU observations during January 2000
1	Crops, Mixed Farming	28819
2	Short Grass	15570
3	Evergreen Needleleaf Trees	1459
4	Deciduous Needleleaf Tree	218
5	Deciduous Broadleaf Trees	4419
6	Evergreen Broadleaf Trees	11253
7	Tall Grass	22444
8	Desert	90797
9	Tundra	123
10	Irrigated Crops	167
11	Semidesert	28876
12	Ice Caps and Glaciers	0
13	Bogs and Marshes	850
14	Inland Water	0
16	Evergreen Shrubs	0
17	Deciduous Shrubs	2134
18	Mixed Forest	3994
19	Interrupted Forest	1263
20	Water and Land Mixtures	43166

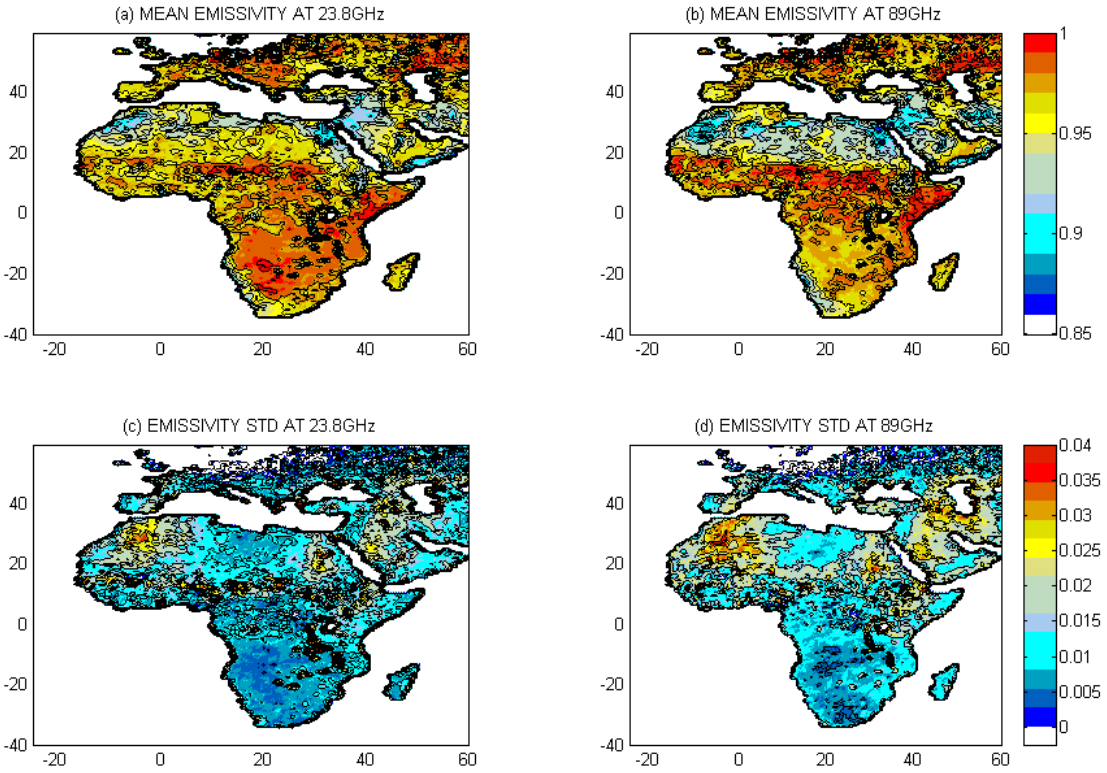

Figure 1: (a) Mean emissivity for July 2000 for low zenith angles (≤ 45°) at 23.8 GHz, (b) same as (a) but at 89 GHz, (c) Emissivity standard deviation for July 2000 for low zenith angles ((≤ 45°) at 23.8 GHz, (d) same as (c) but at 89 GHz.

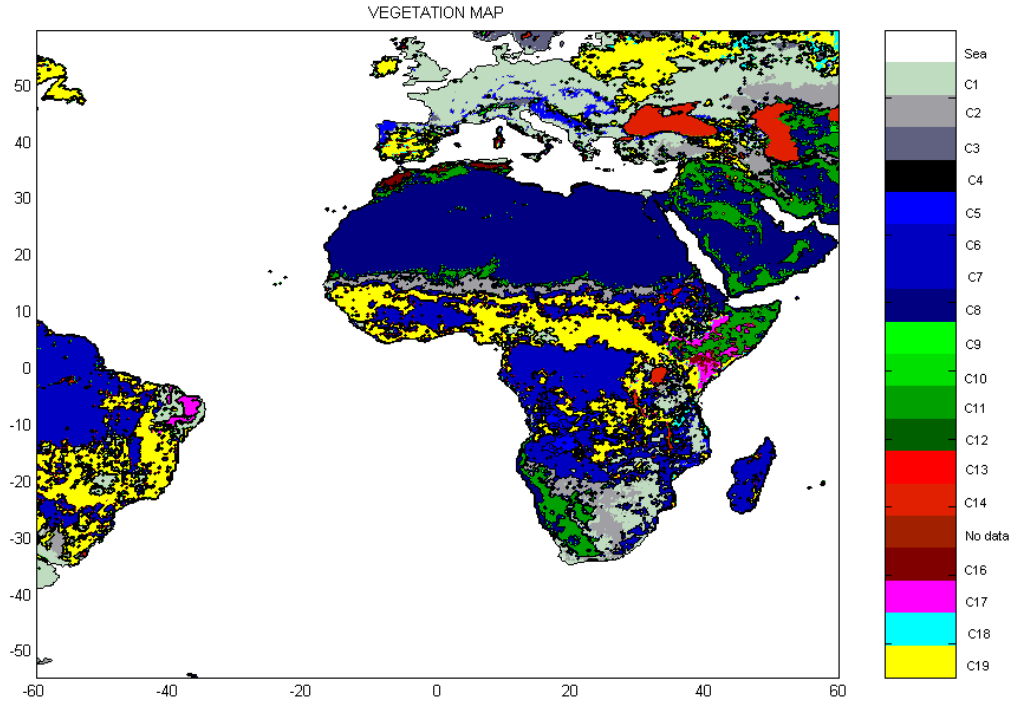

Figure 2: BATS Vegetation classification (see table 3)

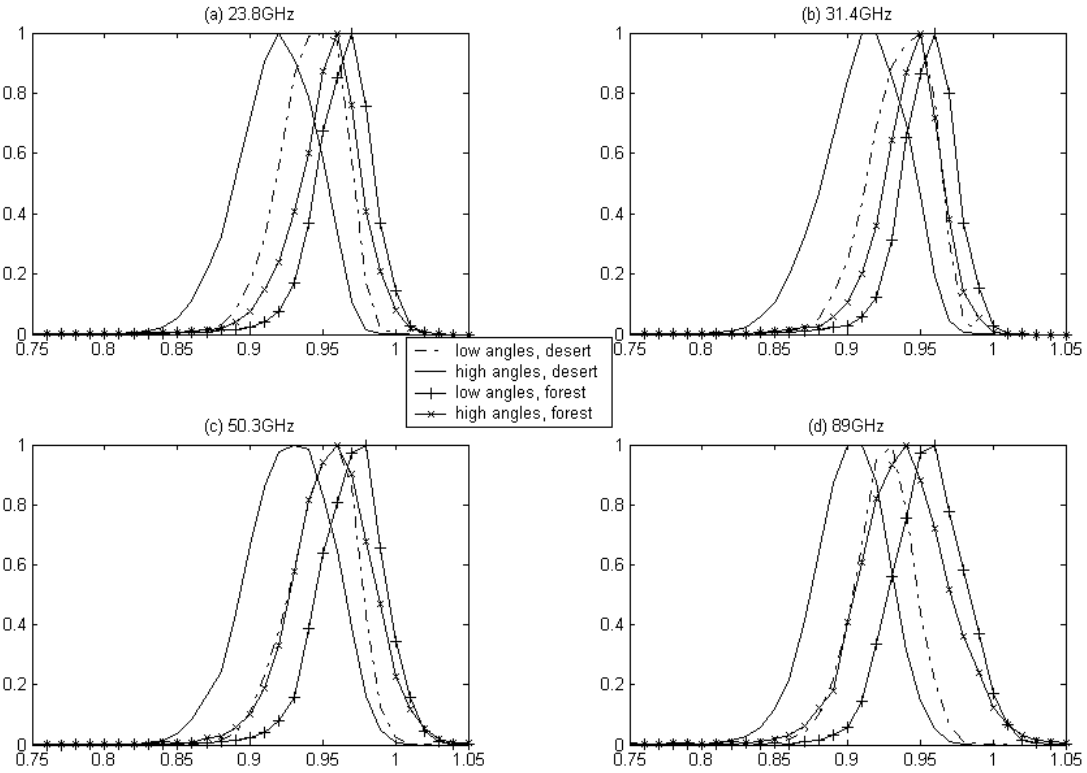

Figure 3: Histograms of the emissivity from February 2000, for low zenith angles and desert (angles ≤ 45°, dashed-dotted curve), for high zenith angles and desert (angles > 45°, solid curve), for low zenith angles and forest (solid curve with plus symbols) and for high zenith angles and forest (solid curve with cross symbols) at (a) 23.8 GHz, (b) 31.4 GHz, (c) 50.3 GHz, and (d) 89 GHz.

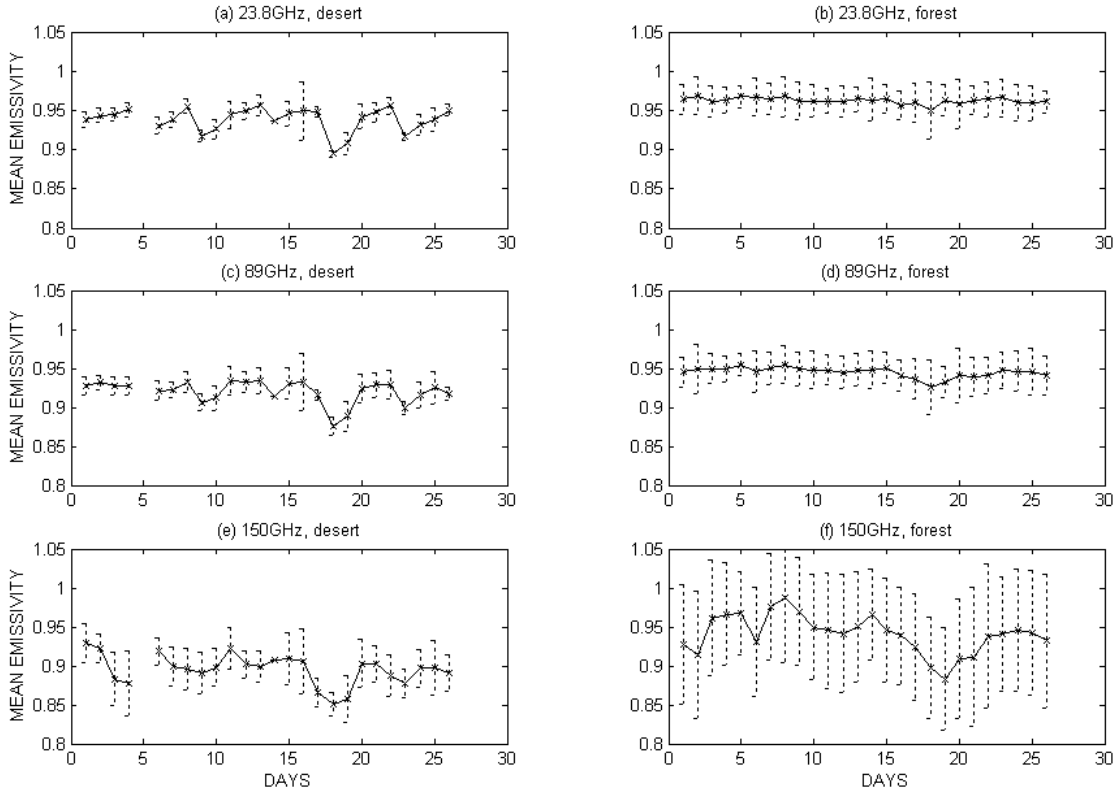

Figure 4: The day-to-day variation of the emissivity over a desert surface at (a) 23.8, (c) 89 and (e) 150 GHz, and over a tropical forest in Africa at (b) 23.8, (d) 89 and (f) 150 GHz.

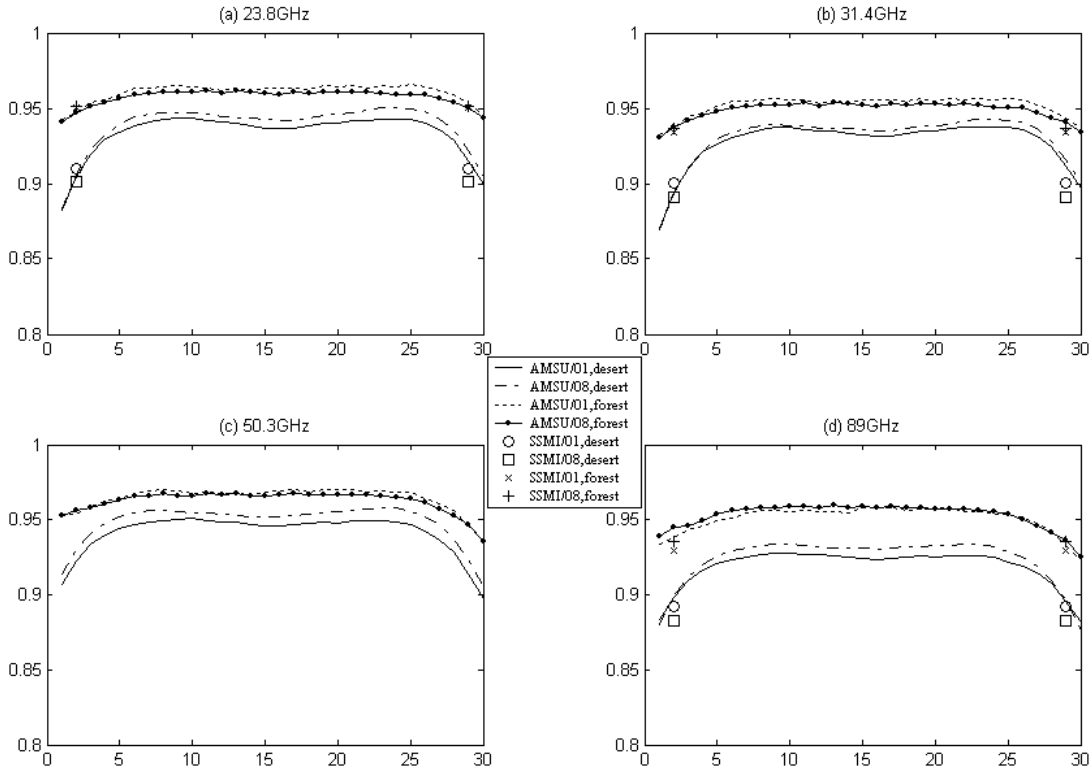

Figure 5: Monthly mean AMSU emissivities with respect to 30 scan positions (±58° of zenith angle variation) and two surface types: desert (solid lines for January and dashed-dotted lines for August) and forest (dotted lines for January and solid-dotted lines for August): (a) at 23.8 GHz with SSMI emissivities at 53° and at 19 GHz, (b) same as (a) but at 31.4 GHz with SSMI emissivities at 37GHz, (c) same as (a) but at 50.3 GHz, (d) same as (a) but at 89 GHz with SSMI emissivities at 85 GHz.

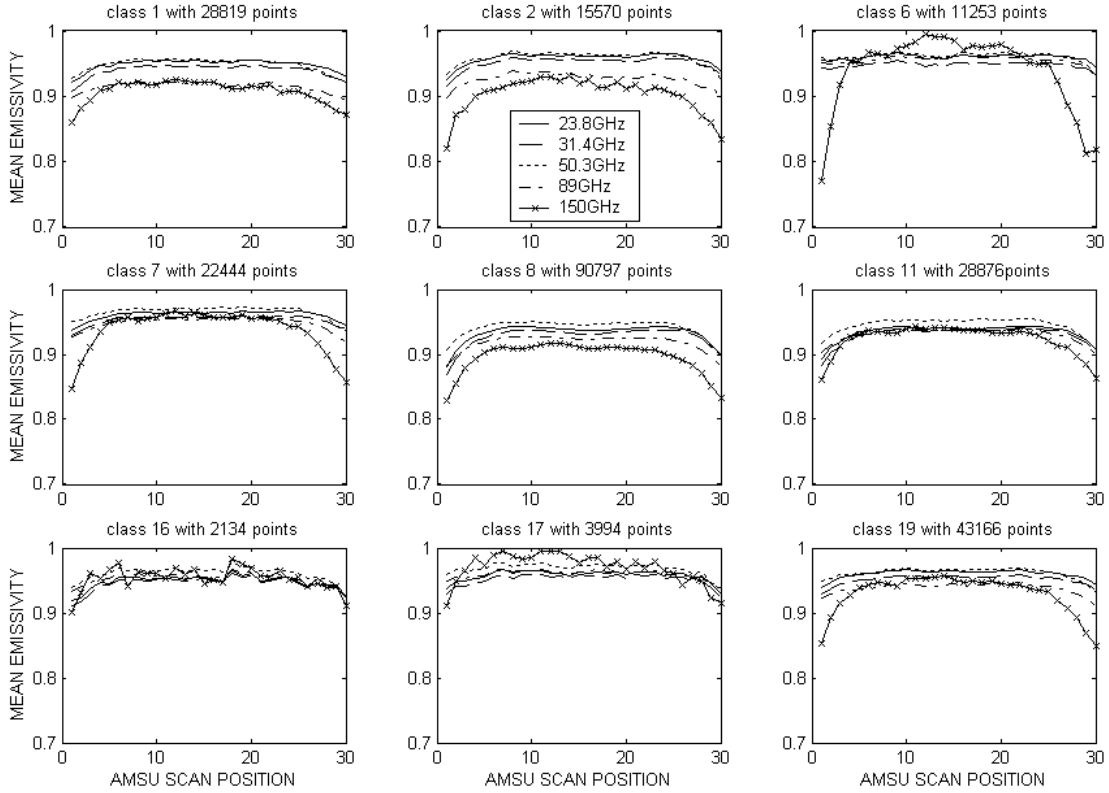

Figure 6: Monthly mean AMSU emissivities for January 2000 with respect to 30 scan positions (±58° of zenith angle variation) and 9 surface types (see table 3 for surface types designation) at 23.8, 31.4, 50.3, 89 and 150 GHz.

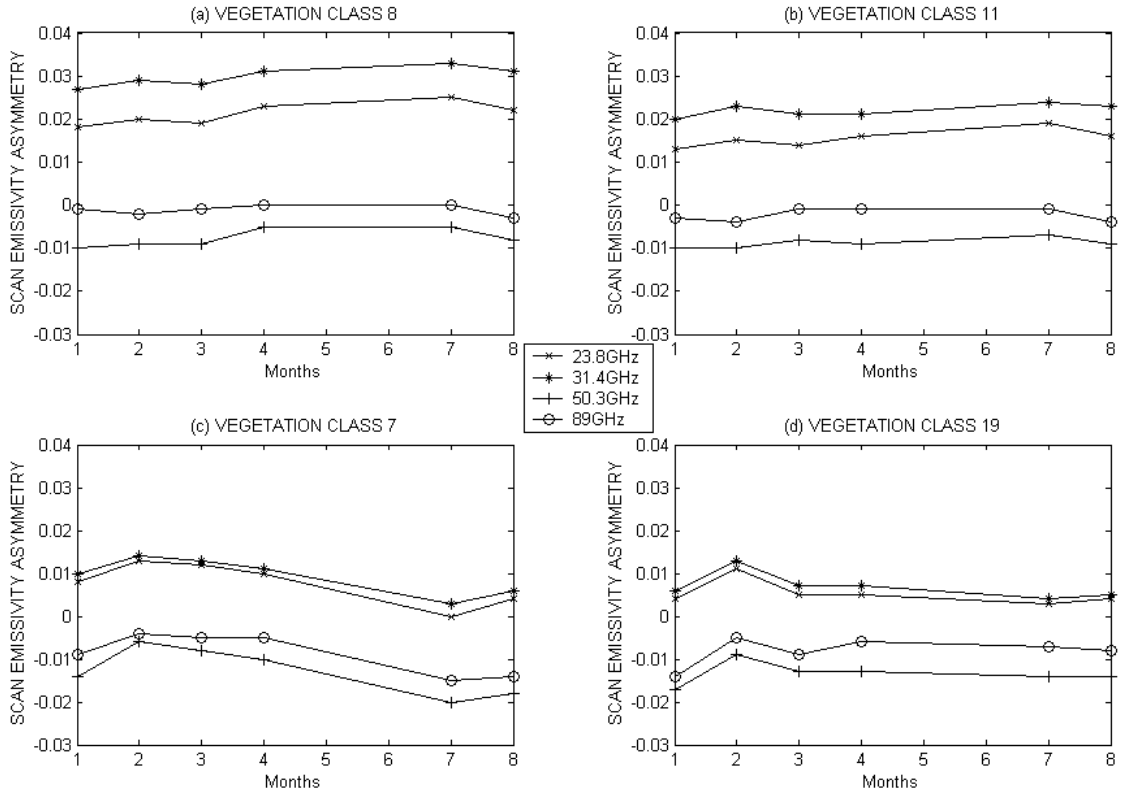

Figure 7: Monthly scan asymmetry (monthly mean emissivity at scan position 30, minus monthly mean emissivity at scan position 1) for 23.8 GHz (solid lines with cross symbol), 31.4 GHz (solid lines with star symbol), 50 GHz (solid lines with plus symbol) and, 89 GHz (solid lines with circle symbol) regarding: (a) vegetation class 8 (desert), (b) vegetation class 11 (semi-desert), (c) and (d) dense vegetation (class 7 and 19).

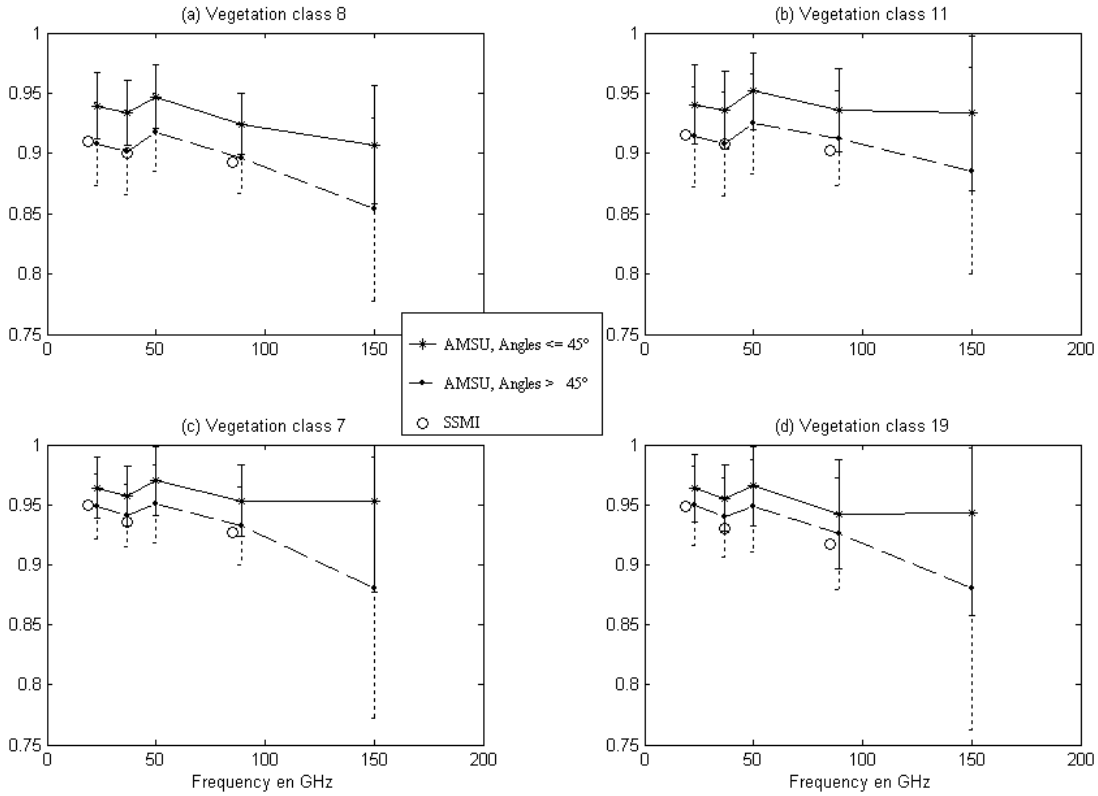

Figure 8: Monthly mean emissivities from January 2000 with respect to the frequency for low zenith angles (≤ 45°, solid lines with star symbols) and high zenith angles (> 45°, solid lines with dot symbol) for (a) vegetation class 8 (desert), (b) vegetation class 11 (semi-desert), (c) vegetation class 7 (evergreen broadleaf trees) and (d) vegetation class 19 (interrupted forest). For each vegetation class, the corresponding SSMI emissivities at 19, 37 and 85 GHz) are added as well as the AMSU emissivity standard deviations.

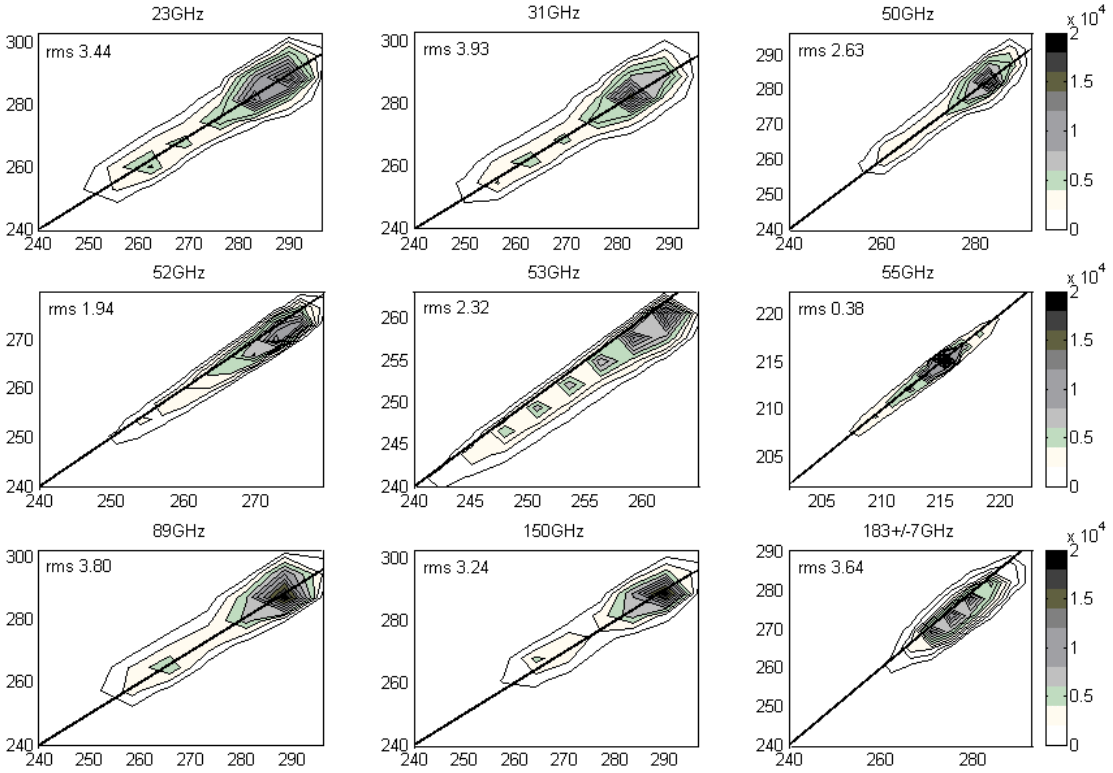

Figure 9: Density contours of the observed brightness temperature (X axis) versus the simulated brightness temperature (Y axis) over land using odd January 2000 days data for AMSU channels 23.8, 31.4, 50.3, 52.8, 53, 89, 150 and 183+/-7GHz. The Root Mean Square (RMS) of (observations-simulations) are added to the plots. The color bar indicates the observations number for each contour class.

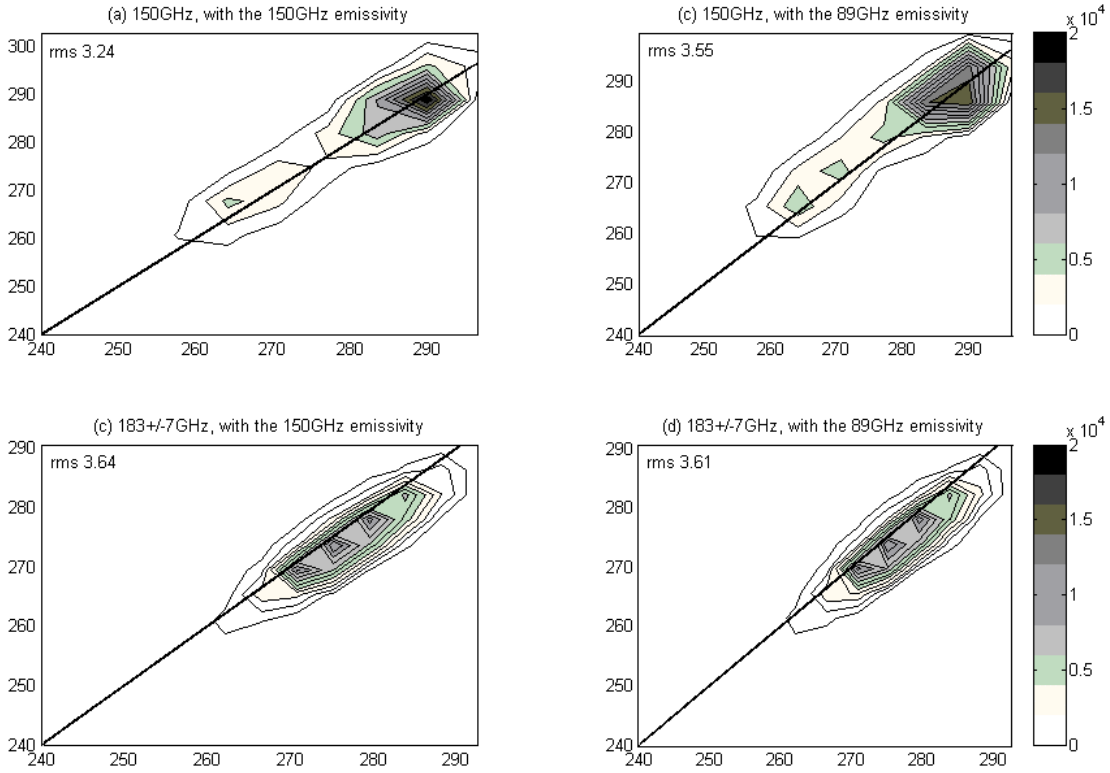

Figure 10: Density contours of the observed brightness temperature (X axis) versus the simulated brightness temperature (Y axis) over land using odd January 2000 days data for AMSU channels: (a) 150 GHz, using the 150GHz emissivity calculated using even January days, (b) 150 GHz, using the 89 GHz emissivity calculated using even January days, (c) same as (a) but for 183±7GHz, (d) same as (c) but for 183±7GHz. The Root Mean Square (RMS) of (observations-simulations) are added to the plots. The color bar indicates the observations number for each contour class.

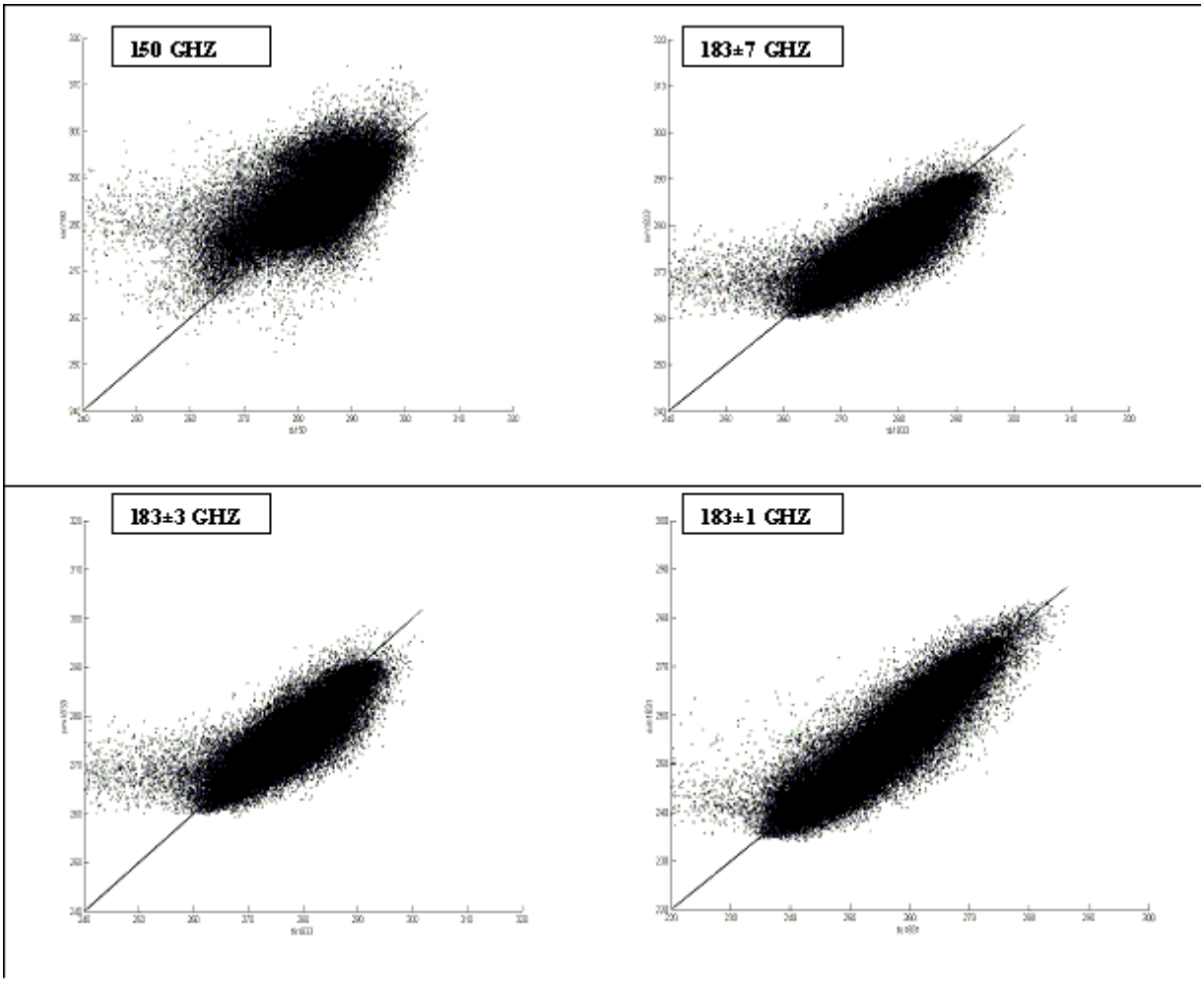

Figure 11: Scatter plots of the observed brightness temperature (X axis) versus the simulated brightness temperature (Y axis) over land using 15 days from August 2000 data for AMSU channels: (a) 150 GHz, using the 89GHz emissivity calculated using July data, (b) same as (a) but for 183±7GHz, (c) same as (a) but for183±3GHz, (d) same as (a) but for 183±1 GHz.